

Magnetic properties of an ensemble of rotating ferromagnetic clusters

N. Hamamoto

Institute of Physics, Graduate School of Arts and Sciences, University of Tokyo, Komaba, Meguro-ku Tokyo 153-8902, Japan

N. Onishi

Department of Ecosocial System Engineering, Yamanashi University, 4-3-11 Takeda, Kofu, Yamanashi 400-8511, Japan

G. Bertsch

Department of Physics and Institute for Nuclear Theory, Box 351560, University of Washington, Seattle, Washington 98195

(Received 2 November 1998; revised manuscript received 12 August 1999)

We analyze the adiabatic magnetization of ferromagnetic clusters in an intermediate-coupling regime, where the anisotropic potential is comparable to other energy scales. We find a nonmonotonic behavior of the magnetic susceptibility as a function of coupling with a peak. Coriolis coupling effects are calculated; they reduce the susceptibility somewhat.

I. INTRODUCTION

Magnetic properties of a wide variety of ferromagnetic clusters, e.g., Fe, Ni, and Co in transition metals involving $3d$ electrons,¹⁻⁴ and Ru, Rh, and Pd associated with $4d$ electrons,^{3,5,6} are studied using the Stern-Gerlach technique. The observed deflection profile, caused by the interaction of magnetization and the gradient of field strength, provides information about these intrinsic magnetic moments of the cluster as well as its coupling to other degrees of freedom in clusters. The size of the cluster is small enough to be regarded as a single-domain system, and the electrons involved form a single giant magnetic moment; we will call it the superelectron spin in this paper. It is quite interesting to see that, in such a low-dimensional system, some elements form ferromagnetic clusters, even though the bulk material is nonmagnetic.⁶ Also, the magnetization is strongly dependent on the number of atoms in the clusters.⁷ The analysis or interpretations of the experimental data have caused significant discussion and are still debated. Therefore, it is important in the present stage of study to establish a method of analysis for extracting the intrinsic magnetic moment from the observed deflection profile, and this is the motivation for the present work.

Let us consider the experimental setup. First, clusters formed by laser evaporation are cooled by helium gas, and then the clusters are expanded to form a molecular beam. In the present study we assume that the clusters are in the thermal equilibrium. The density of clusters in the beam is low, so that the clusters may be assumed to be isolated beyond the equilibration zone. Therefore each cluster stays in a certain quantum state in the beam. Finally, the clusters enter into a Stern-Gerlach magnet and are deflected by the interaction of the gradient of magnetic field and the magnetic polarization of superspin induced by the magnetic field. At the entrance of the magnet, the strength of the field changes gradually in time, and a time-dependent interaction for the superelectron spin causes a transition of the initial quantum state to other quantum states. If the time dependence is sufficiently weak compared with coupling of the spin to other modes, the tran-

sition probability to other modes can be neglected. This is called the adiabatic approximation. In the present work, we calculate the profile and the magnetization with this assumption.

If the electrons were completely decoupled from other degrees of freedom such as rotational motion, the deflection profile would be a flat horizontal distribution independent of the field strength. But this is not actually the case for the observed profiles. A small coupling of the magnetic moment to the internal coordinates of the cluster gives rise to spin relaxation, making the profile different from the flat distribution. Hence it is important to make clear how various couplings produce observed deflection profiles.

The simplest model is superparamagnetism in which the population of the magnetic states is proportional to a Boltzmann factor.⁸ In other words, the cluster rotation plays a role as a heat bath for the superelectron spin in the magnetic field. In a practical analysis for extracting the giant magnetic moment, the Langevin formula is widely employed. It assumes equilibrium with a thermal reservoir at a temperature which is the same as the source of the cluster beam. However, it predicts a rather sharp deflection profile which is quite different from the broad profile that is often observed. Hence, the superparamagnetic model seems to be too simple for the analysis of the experiments.

Another simple model is locked-spin model in which the superelectron spin is frozen to the intrinsic orientation of the cluster, which of course is free to rotate.⁹⁻¹¹ This model seems successful in reproducing the small peak observed near the zero deflection angle, which experimentalists call "superparamagnetism." But it is applicable only to Gd clusters and not general. Furthermore, the model ignores the angular momentum of the superelectron spin, which is known to give recoil effects in the Einstein-de Haas effect.

We propose an intermediate-coupling model as a method to extract the giant magnetic moment from the deflection profile.¹¹ This model covers the superparamagnetic and locked-moment models as weak- and strong-coupling limits, respectively. This paper is organized as follows: the intermediate model is explained and formulated in Sec. II, numerical

results of profiles and magnetization are presented for various strength of coupling, strength of magnetic field, and temperature in Sec. III. The conclusions and discussions are presented in Sec. IV.

II. INTERMEDIATE-COUPPLING MODEL

In the present model it is supposed that all the electron spins are aligned in the same direction through the exchange interaction. Thus, the electron spins are in stretched coupling states having a giant total spin $S = \frac{1}{2}n_s N$, where n_s is the number of spins participating the magnetic moment an atom. Since the magnetic moment is proportional to the total spin, the cluster has a single giant magnetic moment expressed as $\mu = g_s S$, in terms of the electronic gyromagnetic ratio g_s .

Consider as a typical case the Fe_{100} cluster at temperature 100 K. According to Kittel,¹² the magnetic moment per atom for the bulk iron is $2.2\mu_B$. Then a spin value of $S \approx 2.2 \times 100 \times 1/2 \approx 100$ and a thermal rotational angular momentum $R \approx 600$ in units of \hbar . These large values of S and R justify a classical treatment of the problem. In fact, in a previous paper¹⁰ the classical treatment allowed the problem to be reduced to a simple and transparent calculation. This was examined for a simple case, by utilizing adiabatic invariance which makes the calculation easy and transparent.

However, in a more general case, in which a fluctuation of spin orientation with respect to the cluster is significant, we are unable to make a simple classical treatment. Furthermore, in the classical treatment, the spin angular momentum is ignored, and thus angular momentum conservation is violated. Since this is a doubtful approximation when S is comparable to R , we follow a fully quantum mechanical treatment.

The formulation of our model is indebted to the theory of deformed nuclei, especially the particle-rotor model; readers who want to know the theory can consult standard textbooks on nuclear structure, e.g., Bohr and Mottelson.¹⁴

Our Hamiltonian H is expressed as a sum of three terms:

$$H = H_{\text{rot}} + H_{\text{coupl}} + H_{\text{mag}}, \quad (1)$$

where the terms are defined as follows. The first term H_{rot} stands for the rotational energy of the cluster which is expressed as

$$H_{\text{rot}} = \sum_{i=1}^3 \frac{\hat{R}_i^2}{2\mathcal{J}_i}, \quad (2)$$

where \hat{R}_i 's represent operators of three angular momentum components referred to the body fixed frame, and \mathcal{J}_i 's express principal moments of inertia. The vibrational modes are not taken into account, because the Debye temperature (for instance, 500 [K] for iron) is much higher than the source temperature. In other words, the rotational motion is considered to work mainly as a heat bath in the spin relaxation.

The second term H_{coupl} expresses a coupling potential between the cluster and the superelectron spin, which originates from the crystal magnetic anisotropy energy caused by molecular or crystal fields. The simplest form of the energy is the uniaxial magnetic anisotropy which, has already been examined in Ref. 11. Here we assume that the clusters have

an internal cubic structure and the potential has cubic symmetry. This is true for the observation of the direction of easy magnetization being [100], [010], and [001] for iron and nickel. The anisotropy constant is measured in the form

$$E_\alpha = K_1(\alpha_1^2\alpha_2^2 + \alpha_2^2\alpha_3^2 + \alpha_3^2\alpha_1^2) + K_2\alpha_1^2\alpha_2^2\alpha_3^2 + \dots, \quad (3)$$

where α_i 's express the direction cosines of superelectron spin. The measured values in the bulk are $K_1 = 36$ [mK/atom] and $K_2 = 13$ [mK/atom] for iron, and $K_1 = -4$ [mK/atom] and $K_2 = 0$ [mK/atom] for nickel. We consider only the first term in the present calculation. In order to formulate the anisotropic interaction, let us start with the above classical picture for angular momentum variables, in which S_i' 's commute:

$$\begin{aligned} H_{\text{coupl}} &= 8uS'^4 \left(\alpha_1^2\alpha_2^2 + \alpha_2^2\alpha_3^2 + \alpha_3^2\alpha_1^2 - \frac{1}{5} \right) \\ &= -u \left\{ S_1'^4 + S_2'^4 + S_3'^4 - 6(S_1'^2S_2'^2 + S_2'^2S_3'^2 + S_3'^2S_1'^2) \right. \\ &\quad \left. + \frac{3}{5}(S_1'^2 + S_2'^2 + S_3'^2)^2 \right\} \\ &= -uS'^4 \sqrt{\frac{32}{35}} \left\{ C_4^{(4)}(\hat{S}) + C_{-4}^{(4)}(\hat{S}) + \sqrt{\frac{14}{5}}C_0^{(4)}(\hat{S}) \right\}. \end{aligned} \quad (4)$$

Here $C_\mu^{(\lambda)}(\hat{S})$ stands for the spherical harmonic proportional to $Y_{\lambda\mu}(\hat{S})$; S_i' is the spin component with respect to the three axes in the body-fixed frame, S_i denotes the spin component referred to the laboratory system, and $u = 2K_1/n_s^4N^3$. The electron spin prefers the direction of fourfold axes of the cubic symmetry. When the direction of the spin is along the fourfold axes, the value of H_{coupl} has a minimum energy $-\frac{8}{5}uS'^4$. And when the direction of the spin is along the eight axes of $(\pm 1/\sqrt{3} \pm 1/\sqrt{3} \pm 1/\sqrt{3})$ represented by the body-fixed coordinate, the value of H_{coupl} turns out to be the energy maximum $\frac{16}{15}uS'^4$. In the quantum Hamiltonian, S' are operators and we are interested in their matrix elements. The reduced matrix element obtained through the Wigner-Eckart theorem is expressed by

$$\langle S || [\hat{S}]^L || S \rangle = \left(\frac{1}{2} \right)^L \sqrt{\frac{(2S+L+1)!}{(2S-L)!}}. \quad (5)$$

For example, for $L=1$, one obtains the familiar form $\sqrt{S(S+1)(2S+1)}$. interaction between the rotor and the superelectron spin in Eq. (4) is given by

$$H_{\text{coupl}}(S, \Omega) = \sum_{\kappa, m} [S^4]_m^4 \mathcal{D}_{m\kappa}^{4*}(\Omega) A_\kappa, \quad (6)$$

where κ takes the values of only 0 and ± 4 and $A_{\pm 4} = \sqrt{5/14}A_0 = -u\sqrt{32/35}$. The wave function of the rotor can

be expanded in terms of the \mathcal{D} functions,¹⁵

$$\phi_{R\mu}(\Omega) = \sum_k f_{Rk} \mathcal{D}_{\mu k}^R(\Omega). \quad (7)$$

Since the Hamiltonian H_{coupl} is scalar, the total angular momentum $\mathbf{I} = \mathbf{R} + \mathbf{S}$ is still a good quantum number for the first two terms of the Hamiltonians, $H_{\text{rot}} + H_{\text{coupl}}$. Accordingly, we select the base labeled by the total angular momentum and magnetic quantum number I_z . The basis is obtained by the angular momentum coupling of the \mathcal{D} function $\mathcal{D}_{\mu k}^R(\Omega)$ and $|S\sigma\rangle$ to $|IM\rangle$. Therefore, the total wave function of the rotor coupled with the superelectron spin is expressed as

$$\Psi_{\nu IM} = \sum_{Rk\sigma} \langle R\mu S\sigma | IM \rangle \mathcal{D}_{\mu k}^R(\Omega) f_{Rk}^{\nu I} |S\sigma\rangle, \quad (8)$$

where ν represents an index specifying states having the same IM . The matrix element of the coupling term between the bases in Eq. (8) is estimated as

$$\begin{aligned} (H_{\text{coupl}})_{Rk, R'k'}^I &= \sqrt{(2R+1)(2S+1)} (-1)^{S+R'-I} \\ &\times A'_\kappa \langle Rk4\kappa | R'k' \rangle W(RS R' S; I4), \quad (9) \end{aligned}$$

where $\sqrt{2S+1} A'_\kappa = A_\kappa \langle S || [\hat{S}]^4 || S \rangle$, and the Racah coefficient $W(abcd; ef)$ is related to the $6j$ symbol.¹⁵

In our calculation we use the potential strength parameter $u' = A'_{\pm 4}$. Now, the wave function (8) and the energy in the source are determined by diagonalizing $H_{\text{rot}} + H_{\text{coupl}}$. Since there remains the $(2I+1)$ -fold degeneracy in energy for M , we may omit M from the label for the energy $E_{\nu I}$.

The third term in Eq. (1) represents the interaction between an external magnetic field and the moments of the superelectron spin:

$$H_{\text{mag}} = -\mathbf{B} \cdot \boldsymbol{\mu} = -Bg_s \hat{S}_z. \quad (10)$$

We choose the direction of the applied magnetic field as the axis of quantization (z axis). This interaction breaks rotational symmetry for the cluster, but the magnetic quantum number M defined above is still conserved due to the choice of quantization axis. From Eqs. (8) and (10), the matrix elements between two states are calculated as

$$\begin{aligned} \langle \Psi_{\nu IM} | H_{\text{mag}} | \Psi_{\nu' I' M} \rangle &= -Bg_s \hbar \sqrt{2I'+1} (-1)^{I'} \\ &\times \langle I' M 10 | IM \rangle h_{\nu I \nu' I'}, \quad (11) \end{aligned}$$

where the M -independent part $h_{\nu I \nu' I'}$ is expressed as

$$\begin{aligned} h_{\nu I \nu' I'} &= \sum_{Rk} f_{Rk}^{\nu I*} f_{Rk}^{\nu' I'} \sqrt{S(S+1)(2S+1)} (-1)^{R-S+1} \\ &\times W(IS I' S; R1). \quad (12) \end{aligned}$$

For simplicity, we set the moment of inertia around the intrinsic axes to take the same value, namely, $\mathcal{I}_1 = \mathcal{I}_2 = \mathcal{I}_3 = \mathcal{I}$. In this case, total wave functions are classified by an additional quantum number $\pi_k = 0, 1, 2, 3$ ($k \bmod 4$), since H_{rot} is diagonal and H_{coupl} couples to only the states having k quantum numbers different by 4. This point is different from uniaxial anisotropy, in which k quantum number is strictly

conserved due to the axial symmetry. The total wave functions in the magnetic field are expressed as

$$|\Phi_{\alpha \pi_k M}(B)\rangle = \sum_{\nu I} F_{\alpha \pi_k M}^{\nu I}(B) |\Psi_{\nu I \pi_k M}\rangle, \quad (13)$$

where α labels the state in the same π_k, M .

To compare with the experiment, we calculate the average magnetization, which we regard as the ensemble average of $\langle \hat{S}_z \rangle$. This is the sum of the product of the expectation value of \hat{S}_z and the occupation probability of each state. Now we proceed ahead with the important assumption that effect of the magnetic field is adiabatic when the cluster passes through a Stern-Gerlach magnet, as the variation of the magnetic field is slow when the cluster enters into and goes out from the Stern-Gerlach magnet. First, the clusters are retained in the source region. In this region, as the cluster ensemble is in thermal equilibrium, the occupation probability of each quantum state is proportional to the Boltzmann factor $\exp(-E_{\nu I \pi_k} / k_B T)$.

The magnetization of each state in Eq. (13) is calculated as

$$S_{z, \alpha(\nu I) \pi_k M}(B) = \langle \Phi_{\alpha(\nu I) \pi_k M} | \hat{S}_z | \Phi_{\alpha(\nu I) \pi_k M} \rangle, \quad (14)$$

where $\alpha(\nu I)$ stands for the label of states connected adiabatically with the states (νI) defined in the absence of a magnetic field.

Under the adiabatic condition, any transition between energy levels does not occur even if a magnetic field is applied. The occupation probability of each quantum state is not altered during the flight. Then the deflection profile is obtained by

$$P(s, B, T) = \frac{1}{Z(T)} \sum_{\nu I \pi_k M} \delta(s - S_{z, \alpha(\nu I) \pi_k M}) \exp\left(\frac{-E_{\nu I \pi_k}}{k_B T}\right), \quad (15)$$

where the partition function $Z(T)$ is given by

$$Z(T) = \sum_{\nu I \pi_k} (2I+1) \exp\left(\frac{-E_{\nu I \pi_k}}{k_B T}\right). \quad (16)$$

The magnetization, the ensemble average $\langle \hat{S}_z \rangle_{\text{en av}}$, is expressed by

$$\langle \hat{S}_z \rangle_{\text{en av}} = \int s P(s, B, T) ds. \quad (17)$$

III. MAGNETIC SUSCEPTIBILITY

Magnetic susceptibility plays an important role in analyzing the experiment in which the magnetic field is so weak that magnetization linearly depends on the magnetic field. Examining the magnetic susceptibility, we can easily compare the present model, locked-moment model, and superparamagnetism. We calculate the magnetic susceptibility for the intermediate-coupling model and discuss weak- and strong-coupling limits in following subsections.

For the present, let us discuss a general expression of magnetic susceptibility. Using the Feynman theorem, we ob-

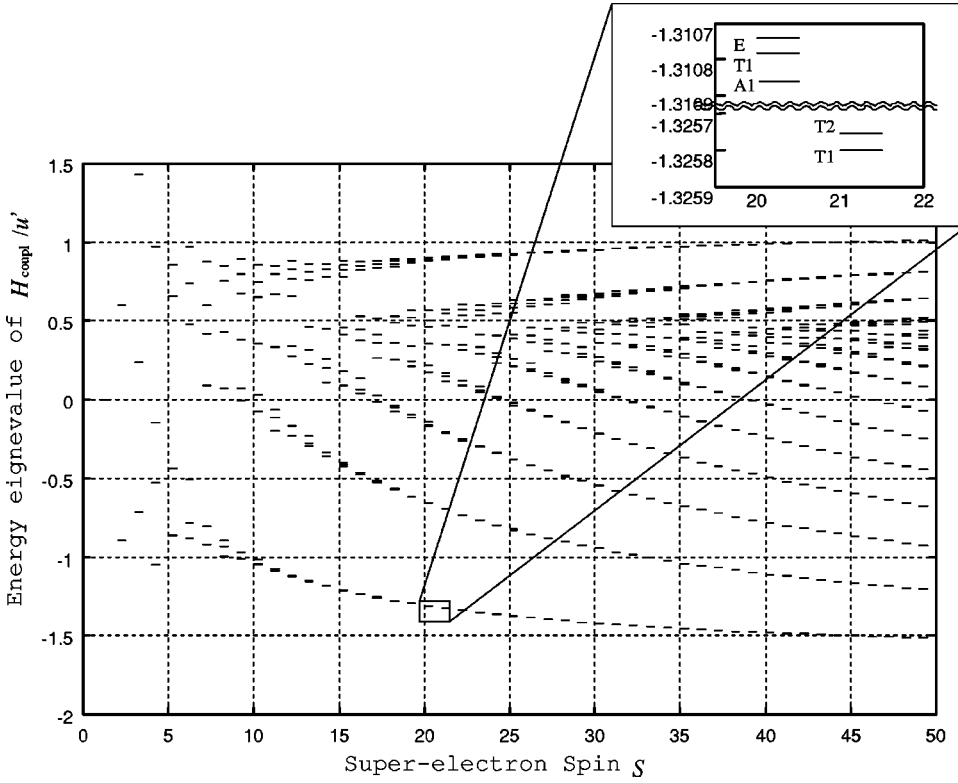


FIG. 1. The eigenvalue of H_{coup}/u' as a function of the magnitude of spin S .

tain the expectation value of S_z as

$$\langle \hat{S}_z \rangle = - \left\langle \frac{\partial}{\partial (B g_s)} H_{\text{mag}} \right\rangle = - \frac{\partial}{\partial (B g_s)} \langle H_{\text{mag}} \rangle. \quad (18)$$

The magnetic susceptibility is expressed as

$$\begin{aligned} \chi &= \frac{\partial}{\partial g_s B} \langle \hat{S}_z \rangle_{\text{en av}} |_{B g_s = 0} \\ &= - \frac{\partial^2}{\partial (B g_s)^2} \Delta E_{\text{en av}} |_{B g_s = 0} \\ &= - \frac{2}{Z(T)} \sum_{\nu I M} \sum_{\nu' I' M'} \frac{|\langle \Psi_{\nu' I' M'} | \hat{S}_z | \Psi_{\nu I M} \rangle|^2}{E_{\nu' I' M'} - E_{\nu I M}} \exp\left(-\frac{E_{\nu I M}}{k_B T}\right), \end{aligned} \quad (19)$$

where $\Delta E_{\text{en av}}$ means the ensemble average of energy shift and partition function.

We will deal with the strong and weak coupling limits of the susceptibility (19) in Secs. III A and III B, respectively. The susceptibility in intermediate coupling will be calculated numerically in Sec. III C.

A. Susceptibility for strong coupling

We first discuss the energy eigenvalue and the eigenstate of $H_{\text{rot}} + H_{\text{coup}}$ in the strong-coupling limit. Since the good quantum numbers are total angular momentum I and its projection on the z axis, M , we rewrite the Hamiltonian of the present model in terms of the total angular momentum I ,

$$\frac{\hat{I}^2 + \hat{S}'^2 - 2\hat{I} \cdot \hat{S}'}{2\mathcal{J}} + H_{\text{coup}}(\hat{S}'). \quad (20)$$

The third term of the numerator is the Coriolis term, which couples the degrees of freedom of superelectron spin to the one of the rotor. It must be noticed that the Coriolis term is not taken into account in the locked-moment model in which the superelectron spin is not included as a dynamical variable. We will be seen how this term contributes to the magnetic susceptibility.

Since H_{coup} gives the dominant contribution to the energy eigenvalue of $H_{\text{rot}} + H_{\text{coup}}$ in the strong-coupling limit, the Coriolis term can be treated by perturbation theory. Without the Coriolis interaction, the unperturbed state is given as a direct product of the eigenfunction of H_{coup} with respect to the intrinsic frame and the eigenfunction of the total angular momentum and its z component: $\mathcal{D}_{MK}^I(\Omega) \Sigma_{\sigma_k} g_{\sigma_k} |S \sigma_k\rangle$. The energy eigenvalues of the Hamiltonian neglecting the Coriolis term are expressed as

$$\frac{\hbar^2}{2\mathcal{J}} [I(I+1) + S(S+1)] + u' E_N^A, \quad (21)$$

where $u' E_N^A$ stands for the energy eigenvalue of the coupling Hamiltonian H_{coup} . This energy spectrum is the rotational band of bandhead energy $u' E_N^A$. For the strong-coupling limit, bandhead of excited bands is much higher than the one of the ground band. The occupation probability of the higher bands can be negligible. We assume that the susceptibility is described by the ground band only. This point will be discussed more closely in Appendix A.

Let us now focus on the ground band of the present model in the strong-coupling limit. Figure 1 illustrates the energy eigenvalues of H_{coup} evaluated numerically in the space $|S \sigma\rangle$: E_N^A . The eigenstate of H_{coup} must belong to a certain irreducible representation of the point group O . The irreducible representations A_1, E, T_1 for $S=4n$, A_2, E, T_2 for S

$=4n+2$, and T_1, T_2 for odd S appear in the lowest-energy region. Considering the dimension of these representations, namely, 1, 1, 2, 3, and 3 for A_1, A_2, E, T_1 , and T_2 , respectively, we find that the bunch of levels always contains six states. The sixfold and eightfold approximately degenerate states appear at the lowest and highest energies, respectively. This fact implies that the direction of superelectron spin is localized to the six (eight) directions corresponding to the potential minima (maxima) in the lowest (the highest) bunching states for large S . Therefore, these states are approximated by

$$\hat{R}^i|SS\rangle, \quad (22)$$

where \hat{R}^i stands for the operator corresponding to the rotation from the third axis to the i th direction of the potential minima.

For the present, we shall take into account the Coriolis term in first-order perturbation theory. According to the first-order perturbation theory of degenerate states, we should solve the secular equation in order to determine the energy shift and perturbed states. In this case, each level in the rotational band is $6(2I+1)^2$ -fold degenerate: The quantum numbers M, K have the values $-I \leq M \leq I$ and the ground state of superelectron spin is sixfold degenerate. The dimension of the secular equation is reduced by a factor of $(2I+1)$ because M is a good quantum number. As we discussed before, the direction of superelectron spin corresponds to the one of the potential minima for the ground state. Choosing the direction of quantization axis as one of the potential minima, we can express the Coriolis term as

$$\hat{I} \cdot \hat{S} = \hat{I}_3^i \hat{S}_3^i + (\hat{I}_+^i \hat{S}_-^i + \hat{I}_-^i \hat{S}_+^i), \quad (23)$$

where

$$\begin{aligned} \hat{I}_3^i &= \hat{R}^i \hat{I}_3 \hat{R}^{i\dagger}, & \hat{I}_\pm^i &= \hat{R}^i \hat{I}_\pm \hat{R}^{i\dagger}, \\ \hat{S}_3^i &= \hat{R}^i \hat{S}_3 \hat{R}^{i\dagger}, & \hat{S}_\pm^i &= \hat{R}^i \hat{S}_\pm \hat{R}^{i\dagger}. \end{aligned}$$

The second term of Eq. (23) does not contribute to the Coriolis matrix element between parallel, antiparallel, or orthogonal directions. In fact, we can estimate the matrix element of raising and lowering operators of superelectron spin:

$$\langle SS | \hat{S}_\pm \hat{R}'(\theta) | SS \rangle = \begin{cases} 0, & \text{for } \theta = 0, \\ \alpha \hbar \sqrt{2S} (1/2)^{S+1}, & \text{for } \theta = \frac{\pi}{2}, \\ 0, & \text{for } \theta = \pi, \end{cases} \quad (24)$$

where $\hat{R}'(\theta)$ is the rotation through angle θ about the axis perpendicular to the three-axis. In addition, the first term of Eq. (23) does not contribute to the matrix element between orthogonal and antiparallel directions, because the matrix elements of \hat{S}_3^i for orthogonal and antiparallel directions are evaluated as $(1/2)^S$ and 0, respectively:

$$\langle SS | \hat{R}'(\theta) | SS \rangle = \begin{cases} 1, & \text{for } \theta = 0, \\ \alpha (1/2)^S, & \text{for } \theta = \frac{\pi}{2}, \\ 0, & \text{for } \theta = \pi. \end{cases} \quad (25)$$

The Coriolis matrix element does not vanish only between parallel directions. Therefore, the secular equation for the Coriolis term is approximately solved. The wave function results in an eigenstate of \hat{I}_3^i :

$$|IMKi\rangle = \hat{R}^i |SS\rangle \hat{R}^i \sqrt{\frac{2I+1}{8\pi^2}} \mathcal{D}_{MK}^I(\Omega). \quad (26)$$

The first-order energy shift is obtained as

$$\langle I'MK'j | 2\hat{I} \cdot \hat{S} | IMKi \rangle = 2\hbar^2 KS \delta_{K,K'} \delta_{I,I'} \delta_{i,j}. \quad (27)$$

We calculate the susceptibility for the strong-coupling limit supposing the wave function of the ground band to be Eq. (26). A detailed account of the derivation of the susceptibility will be described in Appendix A. We obtain

$$\chi = \frac{2}{9} \frac{\hbar^2 S^2}{k_B T} \left(1 - \frac{2}{5} \beta' S^2 + \frac{4}{35} (\beta' S^2)^2 + \dots \right) < \frac{2}{9} \frac{\hbar^2 S^2}{k_B T}, \quad (28)$$

where $\beta' = \hbar^2/2\mathcal{J}k_B T$. The leading order corresponds to susceptibility for the locked-moment model. The higher orders mean correlations through the Coriolis term, in other words, a recoil effect due to the angular momentum of the superelectron spin or Einstein–de Haas effect. We find from Eq. (28) that this effect always suppresses the magnetic susceptibility compared with the one of the locked moment. This fact is apparently seen in numerical calculations in Sec. III C.

B. Susceptibility for weak coupling

In this subsection we calculate the susceptibility for the weak-coupling and high-temperature limits. First, we discuss the energy eigenvalue and the eigenfunction of $H_{\text{rot}} + H_{\text{coupl}}$ in the weak-coupling limit. In the absence of coupling, the energy eigenvalues form a single rotational band with $(2R+1)^2$ -fold degeneracy. The coupling is treated as first-order perturbation theory; the energy shift and wave function are determined by solving the secular equation in a set of degenerate states. Since the degenerate levels in the rotational band split up under the influence of the weak coupling, the energy eigenvalues are expressed as

$$\frac{\hbar^2 R(R+1)}{2\mathcal{J}} + \Delta E_{I\lambda(R)}, \quad (29)$$

where $\lambda(R)$ specifies the state connected adiabatically with R , and $\Delta E_{I\lambda(R)}$ stands for the energy shift in the eigenvalue of the weak anisotropic coupling. The perturbed wave function is expressed as

$$\Psi_{\lambda(R)IM} = \sum_{k\sigma\mu} \langle R\mu S\sigma | IM \rangle \mathcal{D}_{\mu k}^R(\Omega) c_k^{\lambda(R)} | S\sigma \rangle, \quad (30)$$

where the coefficient $c_k^{\lambda(R)}$ is determined by the diagonaliza-

tion of H_{coupl} in the degenerate levels in each R .

We calculate, by employing the Eq. (19), the magnetic susceptibility for weak coupling in the form of a second-order correction to the energy. The energy denominator between the levels in different R is much larger than the one in

the same R in the weak-coupling limit. Thus, we neglect the mixing of states in different R in the limit. The matrix element of Zeeman interaction between the weak-coupling bases, Eq. (30), can be calculated using the orthogonality condition $\sum_k c_k^{\lambda(R)*} c_k^{\lambda'(R)} = \delta_{\lambda\lambda'}$ as

$$\langle \Psi_{\lambda(R)IM} | \hat{S}_z | \Psi_{\lambda'(R)I'M} \rangle = \hbar^2 \delta_{\lambda,\lambda'} \sqrt{2I'+1} (-1)^{I'} \langle I'M10 | IM \rangle \sqrt{S(S+1)(2S+1)} (-1)^{R-S+1} W(II'S;R1). \quad (31)$$

The substitution of Eqs. (29) and (31) into Eq. (19) yields

$$\chi = -\frac{2}{Z(T)} \sum_R \left(\sum_{\lambda(R)MI \neq I'} \frac{|\langle \Psi_{\lambda(R)IM} | \hat{S}_z | \Psi_{\lambda(R)I'M} \rangle|^2}{\Delta E_{I\lambda(R)} - \Delta E_{I'\lambda(R)}} e^{(-E_R + \Delta E_{I'\lambda(R)})/k_B T} \right), \quad E_R = -\frac{\hbar^2 R(R+1)}{2\mathcal{J}}. \quad (32)$$

Since $\Delta E_{I'\lambda(R)}$ is small due to the weak coupling, we can approximate $e^{-\Delta E_{I'\lambda(R)}/k_B T}$ to $1 - \Delta E_{I'\lambda(R)}/k_B T$. Rearranging the summation, we have a form of the susceptibility being independent of dynamics,

$$\chi \approx -\frac{2}{Z(T)} \sum_R \left(\sum_{\lambda(R)MI > I'} \frac{|\langle \Psi_{\lambda(R)IM} | \hat{S}_z | \Psi_{\lambda'(R)I'M} \rangle|^2}{k_B T} \right) e^{-E_R/k_B T}. \quad (33)$$

Putting Eq. (31) into Eq. (33), and expanding for R , we obtain the magnetic susceptibility

$$\chi \approx 2 \frac{\sum_{R=0}^{\infty} \hbar^2 \left(\frac{4S(S+1)(2S+1)R^2}{9} + \dots \right) \exp\left(-\frac{\hbar^2 R(R+1)}{2\mathcal{J}k_B T}\right)}{\sum_{R=0}^{\infty} [(2R+1)^2(2S+1)] \exp\left(-\frac{\hbar^2 R(R+1)}{2\mathcal{J}k_B T}\right)}. \quad (34)$$

At the high-temperature limit, one can evaluate Eq. (34), treating R as a continuous variable and replacing the sum by an integral:

$$\chi \approx \frac{2\hbar^2 S(S+1)}{9k_B T}. \quad (35)$$

It is observed in this subsection that the susceptibility of the weak-coupling limit coincides with the one of the locked moment. One should note that this does not mean that the superelectron spin is locked in the weak-coupling limit. The susceptibility is independent of the dynamics in the weak-coupling limit, whereas in the strong-coupling limit the susceptibility originates from the locked-moment dynamics. In fact, taking into account the axial deformation, we find that the susceptibilities of the weak and strong-coupling limits are different. The matrix element of \hat{S}_z is independent of the deformation, because Eq. (31) is independent of λ . The energy level is dependent on the axial deformation. In Eq. (33) the energy dependence in the Boltzmann factor in the numerator is canceled by the partition function in the denominator for the high-temperature limit. Thus, the susceptibility in the weak-coupling limit is independent of the axial deformation. In the strong-coupling limit, the energy level for the ground band is dependent on the deformation apart from the Coriolis term. The matrix element of \hat{S}_z for axial deformed clusters coincides with the spherical one, and depends on the deformation. Thus, the magnetic susceptibility of the strong coupling is dependent on the axial deformation.

Therefore, considering the axial deformation, we find that the susceptibilities for the weak- and strong-coupling limits are different. The two limits happen to be the same value when the value of \mathcal{J}_i 's are equal.

C. Intermediate coupling

We calculate the magnetic susceptibility for intermediate coupling in this subsection. In numerical calculations of the deflection profile and the magnetization, a main task is diagonalization of Hamiltonian matrices of large dimensions. In the source area, the partial Hamiltonian H_{mag} is zero, and therefore the total angular momentum is conserved. The most major population of angular momentum is $I_{\text{eff}}(T) = \sqrt{2\mathcal{J}k_B T/\hbar^2}$ for the rotational band with $(2I+1)^2$ -fold degeneracy. The dimension of matrices to be diagonalized is approximately $S \times I_{\text{eff}}(T)$. A typical size is of the order of 10^5 . In the magnetic field where states having $I/2$ different are mixed, the number of dimensions is magnified by $I/2$, and becomes eventually of the order of 10^7 . It may not be feasible in numerical calculations. Let us use a similarity transformation in order to scale down the angular momenta. In Eq. (9), the matrix element is approximated as

$$(H_{\text{coupl}})_{RK,R'K'} \approx A'_\kappa \frac{\sqrt{(2R+1)(2R'+1)}}{2\bar{R}+1} d_{\kappa\mu}^4(\theta_1) d_{\mu 0}^4(\theta_2), \quad (36)$$

with

$$\bar{R} = \frac{R+R'}{2} \quad \text{and} \quad \mu = R' - R, \quad (37)$$

and two angles θ_1 and θ_2 are defined, respectively, as

$$\cos \theta_1 = \sqrt{\frac{\bar{K}}{\bar{R}}} \quad \text{with} \quad \bar{K} = \frac{K+K'}{2}$$

and

$$\cos \frac{\theta_2}{2} = \sqrt{\frac{(\bar{R}-S+I)(S-\bar{R}+I)}{4\bar{R}S}}. \quad (38)$$

These angles are invariant under a scale transformation defined as

$$\begin{pmatrix} r, r' \bar{r} \\ k, k' \bar{k} \\ s, i, m \end{pmatrix} = \eta \begin{pmatrix} R, R' \bar{R} \\ K, K' \bar{K} \\ S, I, M \end{pmatrix}. \quad (39)$$

In a similar manner, the matrix elements given in Eq. (11) are expressed approximately as

$$\begin{aligned} & \langle \Psi_{\nu\pi_KIM} | H_{\text{mag}} | \Psi_{\nu'I'I' \pi_K M} \rangle \\ & \simeq B g_s \sqrt{S(S+1)} \frac{\sqrt{(2I+1)(2I'+1)}}{2\bar{I}} \\ & \times \sum_{RK} f_{RK}^{\nu I * \nu' I'} (-)^{I'-I} d_{0I-I'}^1(\theta_3) d_{I-I'0}^1(\theta_4), \quad (40) \end{aligned}$$

with

$$\cos \theta_3 = \sqrt{\frac{M}{\bar{I}}}, \quad \cos \frac{\theta_4}{2} = \sqrt{\frac{(\bar{I}-S+R)(S-\bar{I}+R)}{4\bar{I}S}}. \quad (41)$$

The two additional angles θ_3 and θ_4 are also invariant under the scale transformation. Eventually these four angles are invariant under the transformation in Eq. (39). The four d functions are all smooth functions of the four angles.

To make \hat{S}^2 invariant under the similarity transformation, Eq. (39), the Planck constant is changed according to η . In other words, we can scale down the angular momentum quantum number by adjusting the Planck constant as

$$\hbar' = \frac{\hbar}{\eta}, \quad s = \eta S. \quad (42)$$

The temperature $k_B T$, the coupling u' , and magnetic field parameter $g_s B \hbar S$, which have dimension of energy, are invariant under the similarity transformation. In the following, the units of these energy parameters are selected as $\hbar^2 S^2 / 2\mathcal{J}$ which is also invariant under the similarity transformation.

We are now ready to calculate numerically the susceptibility in the intermediate-coupling scheme. It is already known by the analysis in Sec. III A that the ground state of H_{coupl} has to be approximately sixfold degenerate states in the strong-coupling limit. It seems reasonable that the ground state is approximately sixfold degenerate for $S_c=10$. The reason for this is based on the numerical diagonalization of

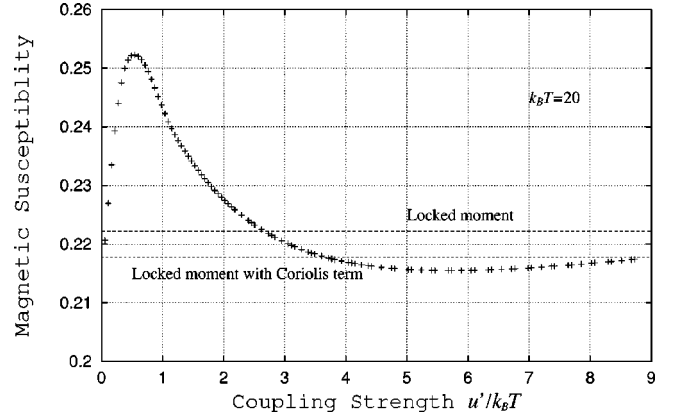


FIG. 2. The magnetic susceptibility calculated by perturbation theory. The ordinate is the coefficient of the magnetic susceptibility χ' (described in the text). The abscissa is the ratio of the coupling strength to temperature.

H_{coupl} in $S_c=10$ (Fig. 1). Three energy levels having onefold, threefold, and twofold degeneracies from lower energy to higher make a bunch around the ground state. The energy differences of these states are about 0.01. In contrast to this, we find from Fig. 1 that the energy difference between the bunch of the ground state and the first excited bunch is about 1.0. The energy spacings between six states around the ground state are much smaller than the energy spacing between the ground bunch and the first excited bunch. Therefore, we can regard the ground state as approximately sixfold degenerate state.

A truncation of the angular momentum is necessary to make numerical diagonalization feasible. We select $I_{\text{max}}=80$ in the calculation. The occupation probability steeply declines as the energy becomes large. For the rotational band, one can neglect states of high angular momentum in the calculation of the partition function. Actually, for the single rotational band with $(2I+1)^2$ -fold degeneracy, levels of which the angular momentum is larger than $I_c(T) = \sqrt{6.2\mathcal{J}k_B T/\hbar^2}$ contribute only less than 10% of the partition function. Therefore the numerical calculation of the partition function is reliable only if $I_c(T) \leq I_{\text{max}}$. For $I_{\text{max}}=80$, the result of the calculation is reliable in its range $k_B T < 20.6$. We choose 20 for the temperature.

We display the coefficient χ' of the magnetic susceptibility obtained by numerical calculation in Fig. 2. The coefficient χ' is defined as

$$\chi = \chi' \frac{\hbar^2 S^2}{k_B T}. \quad (43)$$

We exactly diagonalized $H_{\text{rot}} + H_{\text{coupl}}$, which includes the full Coriolis coupling. Then, the Zeeman coupling H_{mag} is treated as perturbation theory. The first point to be discussed is whether our calculation reaches the two distinct limits discussed above. The susceptibility in Fig. 2 decreases and converges on $2/9$, as the coupling becomes smaller than the temperature. Therefore the result of the calculation is consistent with the analysis for the weak coupling discussed in Sec. III B.

The second point is the strong-coupling limit. As we will discuss in Appendix A, Eq. (A1) is the conditions of tem-

perature and coupling to attain the susceptibility of the locked moment. The application of Eq. (A1) for $S_c=10$ yields the condition of strong coupling:

$$\frac{u'}{k_B T} \gg 3.1. \quad (44)$$

As discussed in Sec. III A, the coefficient of susceptibility for the strong coupling is not the locked-moment value $2/9$ but smaller than it due to the recoil effect. Actually, in Fig. 2, the results of the strong coupling are also smaller than $2/9$ (dashed line), and close to the value of Eq. (28) (dotted line). A possible reason for some deviation from the dotted line is that the quantum fluctuation of the direction of the superspin among different minima of the coupling potential decreases the susceptibility.

A peak at $u'/k_B T \approx 0.55$ is found in Fig. 2. At the peak, the energy splitting of the anisotropic interaction is comparable to the energy splitting by the Coriolis term $(\hbar^2/2\mathcal{J})4SI_{\text{eff}}(T)$. The width of the energy splitting of the anisotropic interaction corresponds to the energy difference between potential maxima and minima, i.e., $\frac{8}{3}u'$. In practice the width becomes smaller due to the quantum fluctuation of the direction of superspin and is found $2u'$ for $S=10$ from Fig. 1. Then the peak is expected to be

$$2u' \approx \frac{\hbar^2}{2\mathcal{J}}4I_{\text{eff}}S \Leftrightarrow \frac{u'}{k_B T} \approx 2 \sqrt{\frac{\hbar^2 S^2}{2\mathcal{J}} \frac{1}{k_B T}} \approx 0.45. \quad (45)$$

In fact, this condition is consistent with the observed position of the peak.

As mentioned in the introduction, one often assumes superparamagnetism, in which the susceptibility is $\frac{1}{3}\hbar^2 S(S+1)/k_B T$, for the clusters to analyze the experiments. We find from Fig. 2 that the superparamagnetic limit is not reached in any range of coupling strength.

The last point is the temperature dependence of the magnetization. It is reasonable to consider that the susceptibility decreases as the temperature increases because of thermal fluctuations of the direction of superspin. In Ref. 1, it was reported that the temperature dependence of the magnetization is reversed. However, in our calculations, such a behavior did not appear in any range of coupling.

IV. PROFILES AND MAGNETIZATION

As mentioned in the previous section, truncation of the angular momentum is necessary to make the numerical calculations feasible. We take $I_{\text{max}}=26$, and the magnitude of superelectron spin $S_c=10$. The result of the calculation is reliable if $k_B T < 2$ for $I_{\text{max}}=26$. Since high temperature is one of the conditions to achieve a locked moment, we should select the temperature as high as possible. Then we choose $k_B T=2$.

First, we pay attention to the magnetic field dependence of the deflection profile. Figure 3 shows the deflection profile for three values of the magnetic field strength $g_s B \hbar S = 0.5, 2, 10$, respectively. Our calculation exhibits that the position of the peak always deflects to the strong-field side, as observed in many experiments. By solving the classical equation of motion, Ballone *et al.* have demonstrated in Ref. 13 that the coupling between the superspin and the cluster

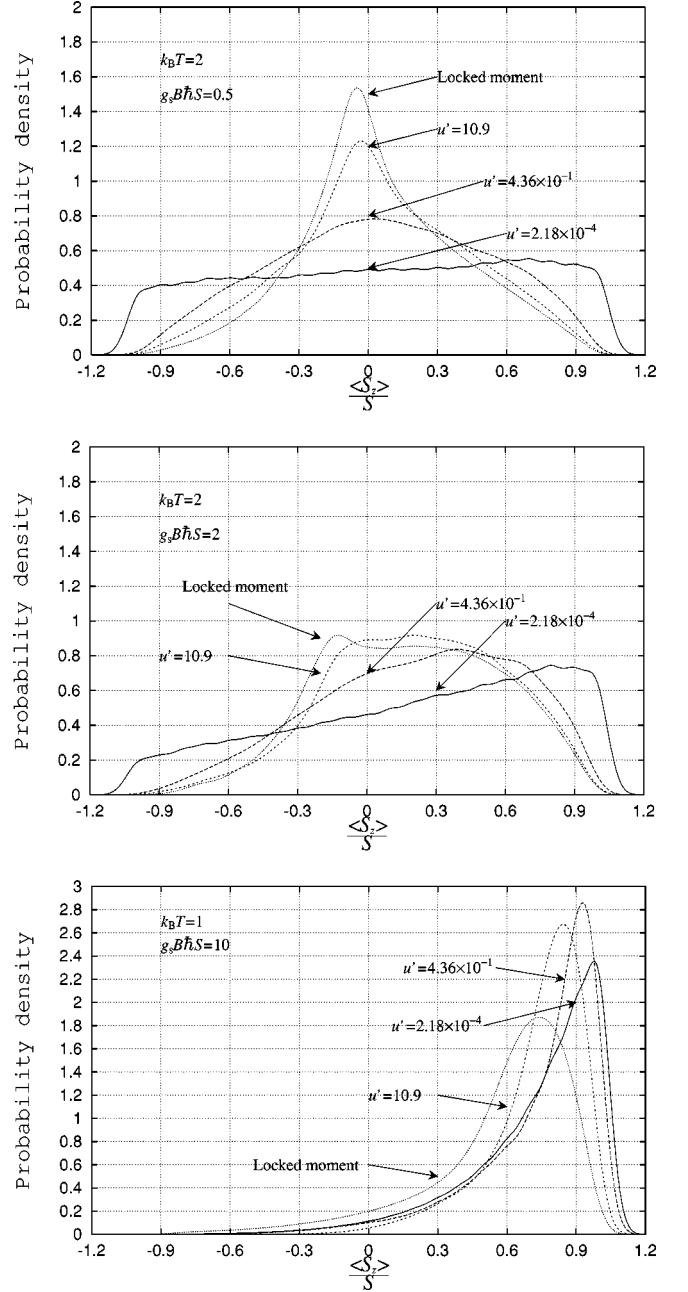


FIG. 3. The profile for three coupling strength $u' = 2.24 \times 10^{-4}$, $u' = 4.47 \times 10^{-1}$, and $u' = 11.2$ of magnetic fields $g_s B \hbar S = 0.5, 2, 10$. The temperature is set to $k_B T = 2$ for $g_s B \hbar S = 0.5, 2$ and to $k_B T = 1$ for $g_s B \hbar S = 10$.

body causes the deflection behavior. We will have a closer examination of this statement in terms of our quantal model.

In order to make our discussion transparent, we start with the weak-coupling limit. The profile of the weak coupling in Fig. 3 is a flat but slightly sloping distribution in the weak magnetic field. Figure 4 showing the energy levels of the weak coupling, $u' = 4.47 \times 10^{-3}$ for $S_c=2$, $M=0$, $\pi_k=0$, and $R \approx 3$ or 4, helps us to understand the distribution in terms of the energy level. In the absence of coupling, the energy levels of the present model form a single rotational band. These levels split up under the influence of the weak coupling; energy levels form a bunch of states around each unperturbed state in the rotational band. As the applied mag-

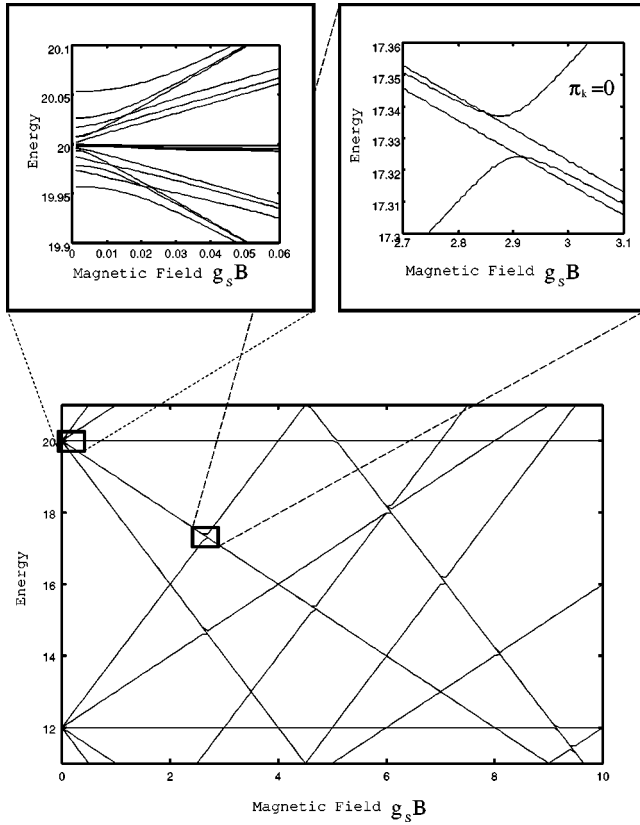


FIG. 4. Energy levels of the weak coupling ($u' = 4.47 \times 10^{-3}$) as a function of magnetic field for $S_c = 2$, $M = 0$, and $R \approx 3$ or 4.

netic field becomes stronger than the coupling, these levels split up again under the influence of the applied magnetic field, and are rearranged more likely to be the eigenfunction of \hat{S}_z . In other words, the superspin precesses about the direction of the magnetic field independently of the cluster (decoupling) for $g_s B \hbar S > u'$. Occupation probabilities of levels in the same R become almost equal due to the weak coupling. Then, the magnetization remains small and the profile becomes a flat distribution. When the energy difference resulting from the Zeeman splitting is equal to a typical energy spacing of the rotational levels, $2g_s B \hbar S = \hbar^2 R_{\text{eff}} / \mathcal{J}$, a pseudocrossing between different rotational levels occurs. In other words, the pseudocrossing takes place where the Larmor precession frequency ω_L is comparable to the cluster rotation frequency ω_{rot} : $\omega_L \approx \omega_{\text{rot}}$. That is to say, the pseudocrossing leads to an exchange of the occupation probabilities between those levels. This process increases the magnetization, and develops a peak in the profile at $\langle S_z \rangle / S = 1$ like the Boltzmann distribution.

The above discussion leads us to divide the mechanisms of magnetization into two types, that is, the magnetizations by the processes of decoupling and by the pseudocrossing. These two types of magnetization are apparently seen in Fig. 5 in which we show the magnetic field dependence of the magnetization in the weak-coupling limit. The magnetization linearly increases as the magnetic field in the process to decoupling, then remains steady by the decoupling of superspin, and finally increases suddenly through the pseudocrossing. In the intermediate- and strong-coupling limits, we cannot distinguish the regions of the magnetic field strength

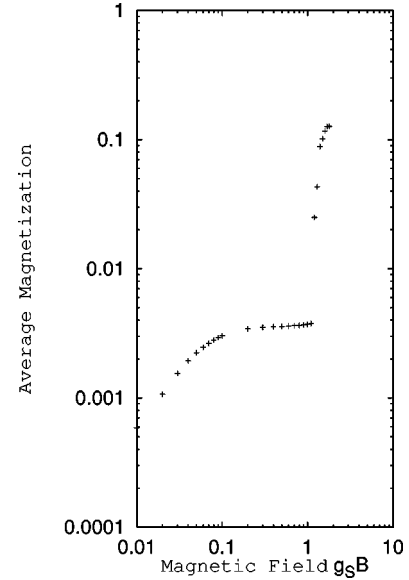


FIG. 5. An example of the peculiar behavior of magnetization for $S_c = 2$.

in which either the decoupling or the pseudocrossing occurs. Accordingly, the peculiar behavior of magnetization observed in the weak-coupling limit disappears.

The calculated susceptibility (Fig. 2) indicates that $u' = 11.2$ is in the strong-coupling region. However, the profile in this case in Fig. 3 is not identical with the locked-moment

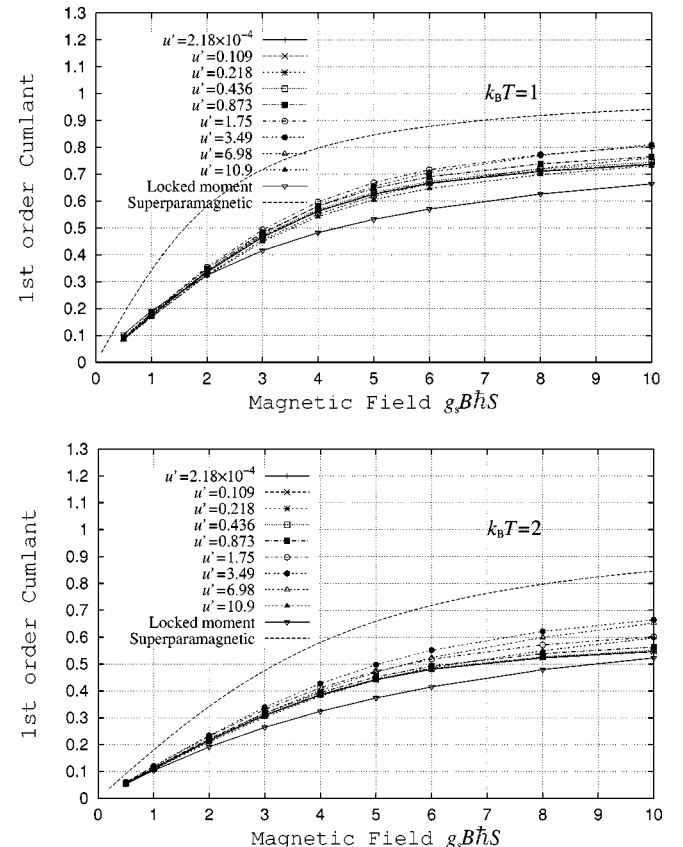


FIG. 6. The first-order cumulant of each profile as a function of the magnetic field $g_s B \hbar S$. The temperature $k_B T$ is fixed at 1 and 2 for (a) and (b), respectively.

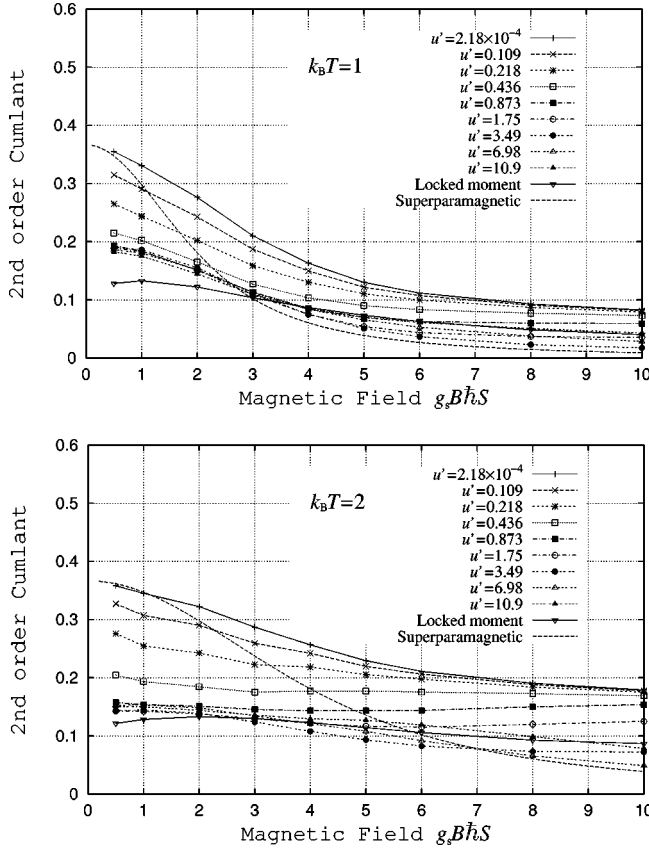


FIG. 7. The second-order cumulant of each profile as a function of the magnetic field $g_s B \hbar S$. The temperature $k_B T$ is fixed at 1 and 2 for (a) and (b), respectively.

profile. We attribute this to the Coriolis term, which is important at the temperature of the ensemble, $k_B T = 2$. A higher temperature was possible in the calculation in Ref. 11 because a simpler anisotropy term there permitted smaller dimension Hamiltonian matrices.

Finally, let us move to the discussion of the profiles in intermediate coupling. We select the cumulants to characterize the profiles. The first- and second-order cumulants mean the average and the variance of the profile, respectively. A cumulant higher than second order vanishes for the Gaussian probability distribution. In our calculation the third- and fourth-order cumulants are less than 10% and 1% of second order, respectively. Thus, the profiles in the intermediate-coupling limit can be approximated by the Gaussian profile.

We now discuss the first- (Fig. 6) and second- (Fig. 7) order cumulant in more detail. The general trend of the first-order cumulant looks like more or less one of either the superparamagnetic or locked moments. The magnetization of intermediate coupling is smaller than the one of the locked moment because of the recoil effect. We may note, in passing, that the anomalous behavior in the weak-coupling limit, discussed earlier, should appear when the energy splitting by the magnetic field is comparable to the typical energy difference of rotational levels, that is,

$$2g_s B \hbar S \approx \frac{2\hbar^2 R_{\text{eff}}}{2\mathcal{J}} \Leftrightarrow g_s B \hbar S \approx \frac{1}{S} \sqrt{\frac{\hbar^2 S^2 k_B T}{2\mathcal{J}}} \approx 0.14. \quad (46)$$

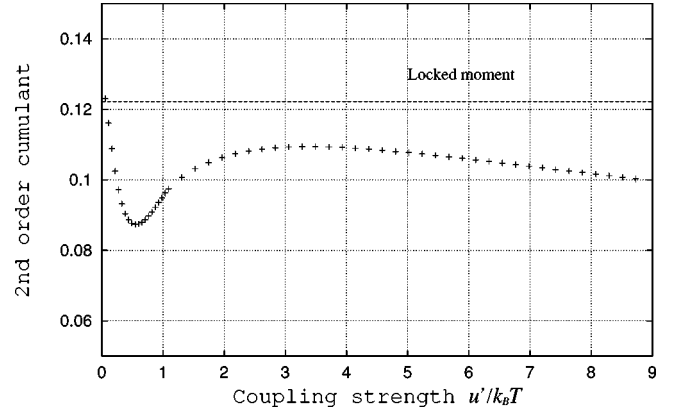


FIG. 8. The second-order cumulant of the profile as a function of the ratio of coupling strength u' and temperature $k_B T$. The temperature is fixed at 20.

But this region is out of the calculated range of Fig. 6.

The second-order cumulant is calculated by means of two methods. One is the direct diagonalization of H , and the other is the perturbation for the magnetic field. Figure 7 illustrates the second-order cumulant, as a function of magnetic field, obtained by direct diagonalization. The second-order cumulant is sensitive to the coupling. The cumulant declines as either the coupling or the magnetic field becomes stronger. In other words, the magnetic field and the coupling make the shape of the profile narrower. The second-order cumulant of the locked-moment profile in the absence of a magnetic field and the flat profile observed in the decoupling region are estimated as $\frac{1}{9}$ and $S(S+1)/3S^2$, respectively. Actually, in Fig. 7, the strong coupling $u' = 10.9$ and the weak coupling $u' = 2.18 \times 10^{-4}$ in the weak magnetic field are close to $\frac{1}{9}$ and $S(S+1)/3S^2$, respectively.

Figure 8 shows the second-order cumulant in the absence of a magnetic field evaluated by perturbation of the magnetic field. The maximum of angular momentum I_{max} and the temperature $k_B T$ are taken at 80 and 20, respectively. The maximum of the angular momentum in this calculation is much larger than the one in the direct diagonalization. The second-order cumulant of the profile approaches the strong-coupling limit $1/9$ in the coupling $u' = 3.5$. It decreases almost linearly in the region of the coupling beyond 20 because of the tunneling between different directions of the potential minima.

For the weak-coupling limit, the ensemble average of the profile converges on 0.122 as seen in Fig. 8. We can estimate the second-order cumulant of the weak-coupling limit. The magnetization of each level in this limit is calculated from the diagonal part of Eq. (31):

$$\langle \hat{S}_z \rangle = \hbar \sqrt{2I+1} (-1)^I \langle IM10 | IM \rangle \sqrt{S(S+1)(2S+1)} \times (-1)^{R-S+1} W(ISIS; R1). \quad (47)$$

The second-order cumulant for weak coupling is estimated to be

$$\begin{aligned}
\langle \hat{S}_z \rangle_{\text{cumulant}}^2 &= \hbar^2 \frac{S(S+1)(2S+1)}{Z(T)} \\
&\times \sum_{RIM\lambda(R)} (2I+1) |\langle IM10|IM \rangle|^2 \\
&\times |W(ISIS;R1)|^2 \exp\left(-\frac{E_R}{k_B T}\right). \quad (48)
\end{aligned}$$

Treating R as a continuous variable and replacing the sums by an integral yields

$$\langle \hat{S}_z \rangle_{\text{cumulant}}^2 \approx \frac{\hbar^2}{9} S(S+1). \quad (49)$$

Actually, in Fig. 8, the second-order cumulant of the profile is close to $S_c(S_c+1)/9S_c^2 \approx 0.122$.

Let us look at Fig. 7 again and discuss the behavior around the flat profile which is seen in the weak-coupling region of the figure. The flat distribution is achieved, as discussed before, in the decoupling region. The magnetic field is much stronger than the coupling, though it is not so strong as to give rise to pseudocrossing between states of different R . Hence, we need two assumptions for calculating the magnetic field or coupling dependence of $\langle \hat{S}_z \rangle^2$ by perturbation of the coupling. The first one is that the magnetic field is much larger than the coupling,

$$g_s B \hbar S \gg u', \quad (50)$$

to assume the decoupling of the superspin from the cluster. The second assumption is that the magnetic field is weaker than the energy difference between the states of different R ,

$$g_s B \hbar S < \frac{\hbar^2}{2J} 2R_{\text{eff}}, \quad (51)$$

which assures us that pseudocrossing does not occur at least for levels having typical angular momentum. A detailed account of the calculation is presented in Appendix B. Here we give just the result, Eq. (B15):

$$\begin{aligned}
\langle \hat{S}_z \rangle_{\text{en av}}^2 &\approx \frac{1}{3} \hbar^2 S(S+1) - \frac{64}{1215} \left(\frac{u'}{B g_s} \right)^2 \\
&+ \left\{ \frac{4}{135} \hbar^2 \left(\frac{-190 + 39S(S+1)}{693} \right) \right. \\
&\left. - \frac{4}{3645} \hbar^2 S(S+1) \right\} \left(\frac{u'}{k_B T} \right)^2. \quad (52)
\end{aligned}$$

When one analyzes the experiment in more detail, the higher-order cumulants may bring about important information. For example, the third-order cumulant (Fig. 9) characterizes the asymmetry of the profile. In the whole range of magnetic field, the third-order cumulant is smaller than the second-order cumulant and is smaller as the coupling becomes stronger. The profiles are always symmetric with respect to $\langle S_z \rangle = 0$ in the absence of a magnetic field. When the magnetic field is applied, the asymmetry grows on account of time reversal symmetry breaking. The third-order cumulant has a peak at $g_s B \hbar S / k_B T \approx 2$. In a strong magnetic field, the profiles have a narrow peak at $\langle S_z \rangle / S = 1$ like Fig. 3. The

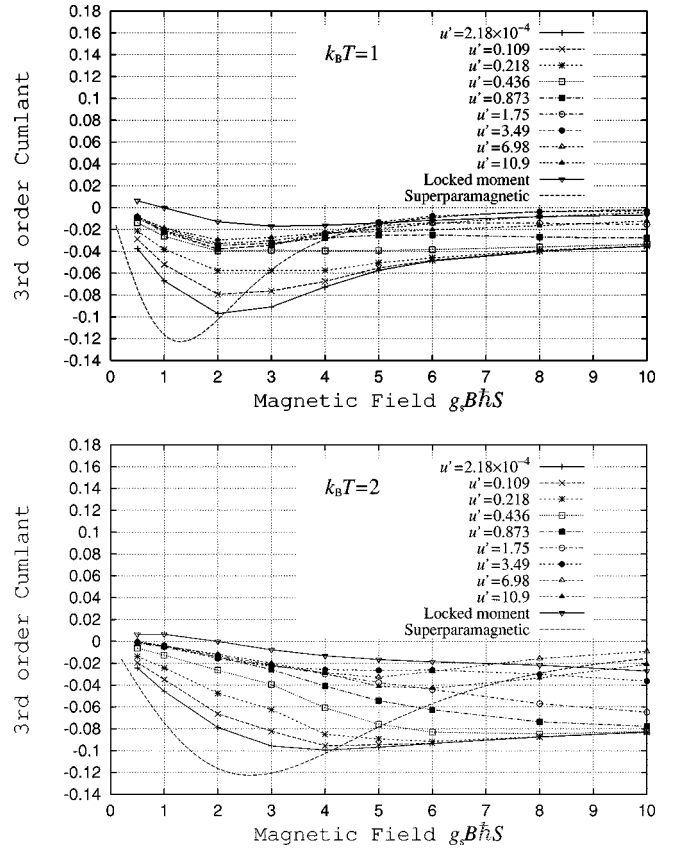


FIG. 9. The third-order cumulant of each profile as a function of the magnetic field $g_s B \hbar S$. The temperature $k_B T$ is fixed at 1 and 2 for (a) and (b), respectively.

profiles are more likely to be symmetric but still not quite. In other words, the third-order cumulant decreases but is not equal to zero.

V. CONCLUSIONS AND DISCUSSION

Using an intermediate-coupling model, we have studied the magnetization of ferromagnetic clusters in a Stern-Gerlach magnet. In this model the superelectron spin is free but couples to the cluster ions through an anisotropic potential. This model is expected to describe the intermediate behavior between the superparamagnetic and the locked moment. In evaluating the profiles or the magnetization, we assume that the variation of the magnetic field in entering the magnet is slow in time, i.e., adiabatic. Hence, any transition between quantum states is suppressed; the occupation probability of each quantum state is determined in the source area where the magnetic field is absent.

We examined the magnetic susceptibility of the present model applying perturbation theory. Especially, the magnetic susceptibility in the strong- and weak-coupling limits is discussed analytically. We expected the intermediate-coupling model to approach the locked-moment behavior in the strong-coupling limit. However, there is a crucial difference between the strong-coupling limit of the present model and the locked-moment model. In the present model the superelectron spin degree of freedom is treated explicitly and the Coriolis term arises due to the conservation of total angular momentum, while in the locked-moment model the Coriolis

term is neglected. Consequently, the magnetic susceptibility is always smaller than the locked moment. The susceptibility in the present model obtained by perturbation theory is not the superparamagnetic value in any range of the coupling.

We find that the irregular magnetic field response noticed in Ref. 11 also exists in the weak-coupling region of the present model. The magnetization linearly increases before the decoupling and saturates after the decoupling. Then, once the pseudocrossing between levels in different R occurs, the magnetization increases again. Before the decoupling, the susceptibility arises as a perturbation of the magnetic field. But after the decoupling, or once the pseudocrossing takes place, the susceptibility becomes nonperturbative. Instead, we need to diagonalize the total Hamiltonian, which is difficult for today's computers for high temperatures and large cutoff angular momentum. Reference 11, including one of the authors (G.B.), discussed the susceptibility after the decoupling using uniaxial coupling. They found that the susceptibility reaches the superparamagnetic value. Therefore, if we were to calculate the susceptibility after the decoupling, the susceptibility would be superparamagnetic.

While an anomalous temperature dependence is reported in Ref. 1, the calculated susceptibility is always positive. We could not reproduce the anomalous temperature dependence.

The "superparamagnetic peak" which is seen in the profile obtained by the locked-moment model is not seen in the present calculation even in the strong-coupling limit. As discussed in Sec. III C, the strong-coupling limit of our model is different from the locked-moment model because of the Coriolis term. It suggests that the effect of the Coriolis term destroys the superparamagnetic peak. If we were able to calculate at such a high temperature that the Coriolis term can be negligible, the peak would appear in the deflection profile.

Finally, we discuss how to analyze the Stern-Gerlach deflection function by our theory. We calculated the cumulant of the profiles up to third order to characterize the profiles. We found from Fig. 6 that the first- and second-order cumulants are dominant. In particular, the evaluation of the susceptibility and second-order cumulant by the perturbation technique gave us the analytical expression of the second-order cumulant and magnetic susceptibility for high temperature and strong or weak coupling. One can extract the magnetic moment and the coupling strength by fitting the observed magnetic susceptibility and the second-order cumulant into the calculated second-order cumulant and the magnetic susceptibility.

For example, we analyzed the experiment for Gd_{23} .³ The experimental temperature is set to $T=5$ [K] according to Ref. 6. Fitting the magnetic susceptibility and second-order cumulant, we extract $1.42\mu_B/\text{atom}$ and 0.185 [K/atom] for the magnetic moment $g_S\hbar S$ and the coupling u' , respectively. The ratio of temperature and magnetic field becomes $g_S B\hbar S/k_B T=0.593$. In Fig. 10, we show the fitted profile and the profile of the locked moment. For both theoretical profiles, the ratios of temperature and the magnetic field are same. The temperature for the present model is set to $k_B T=2$. The profile of the present model makes a better agreement with experiment than the one of the locked moment.

ACKNOWLEDGMENTS

Part of the calculations were performed with a computer VPP500 at RIKEN (Research Institute for Physical and

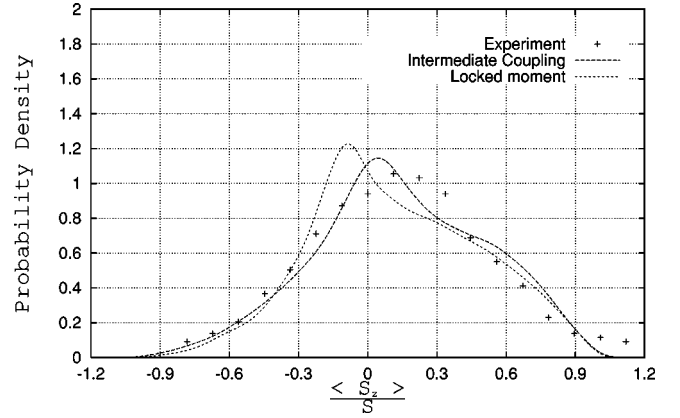


FIG. 10. The profile of experiment and two theoretical models with the same parameter. We set $g_S B\hbar S/k_B T=0.593$ for both theoretical models and $k_B T=2$ for the intermediate-coupling model. The ratio of coupling to temperature, $u'/k_B T$ is set to 0.851.

Chemical Research, Japan) and SX4 at RCNP (Research Center of Nuclear Physics). The authors wish to thank M. Kaneda and Dr. A. Ansari for their helpful advice. We gratefully acknowledge helpful discussions with Dr. N. Tajima especially on the various coupling schemes. One of the authors (N.H.) would like to thank A. Bulgac for letting him participate in the program "Atomic Clusters" (INT-98-2). This work is financially supported in part by a Grant-in-Aid for Finance Research (09640338).

APPENDIX A: THE DERIVATION OF SUSCEPTIBILITY FOR THE STRONG-COUPLING LIMIT

In this appendix, we show the derivation of the susceptibility for the locked-moment limit [Eq. (28)]. In Sec. III A, we supposed that the susceptibility was described by the ground band only. The assumption is valid if the bandhead of excited bands is much higher than the energy of the cutoff level, that is,

$$u'(E_N^A - E_1^A) \gg \frac{\hbar^2 \{I_c(T)\}^2}{2\mathcal{J}}, \quad (\text{A1})$$

where $N \geq 7$ because the ground band consists of sixfold degenerate levels.

The wave function and the energy shift of Coriolis term for the ground band were already discussed and turn out to be Eq. (26) and Eq. (27), respectively. The energy level of the ground band results in

$$E_{IMKi} \approx \frac{\hbar^2}{2\mathcal{J}} [I(I+1) + S(S+1)] + \frac{\hbar^2}{2\mathcal{J}} MK + u' E_i^A \quad (i \leq 6). \quad (\text{A2})$$

The susceptibility is evaluated through Eq. (19) as

$$\chi \simeq -\frac{2}{Z(T)} \sum_{IMKi} \sum_{I'K'i'} \frac{|\langle I'MK'i'|\hat{S}_z|IMKi\rangle|^2}{a[I(I+1)-I'(I'+1)-(MK-MK')]-u'(E_i^A-E_{i'}^A)} \exp\left(-\frac{E_{IMKi}}{k_B T}\right), \quad (\text{A3})$$

where $a = \hbar^2/2\mathcal{J}$. The second term of the energy denominator, $E_i^A - E_{i'}^A$, vanishes because of the sixfold degeneracy of the ground band. The matrix element of \hat{S}_z is evaluated by the wave function of the ground band, Eq. (26),

$$|\langle I'MK'i'|\hat{S}_z|IMKi\rangle|^2 = \delta_{KK'} \delta_{ii'} \hbar^2 S^2 \frac{2I+1}{2I'+1} |\langle IM10|I'M\rangle|^2 |\langle IK10|I'K\rangle|^2. \quad (\text{A4})$$

One should note that the matrix element is same as the one of the locked-moment model.⁹ Substituting Eq. (A4) into Eq. (A3), we get

$$\chi \simeq -\frac{1}{Z(T)} \sum_{IMKi} \sum_{I'} 4\mathcal{J} \frac{S^2 \frac{2I+1}{2I'+1} |\langle IM10|I'M\rangle|^2 |\langle IK10|I'K\rangle|^2}{I(I+1)-I'(I'+1)} \exp\left(-\frac{a\hbar^2[I(I+1)+S(S+1)+2KS]+uE_i^A}{k_B T}\right). \quad (\text{A5})$$

This is different from the susceptibility for the locked moment⁹ only in the Coriolis term. Since the average angular momentum is about $I \approx 600$, one can safely evaluate Eq. (A5), treating I, K as a continuous variable and replacing the sum by an integral. Thus we get

$$\begin{aligned} \chi &\simeq \frac{2\mathcal{J}}{3} \left(1 - \frac{e^{-\beta' S^2}}{S} \int_0^S e^{\beta' t^2} dt\right) \\ &= \sum_{n=0}^{\infty} \frac{2\mathcal{J}}{3\hbar^2} \frac{(-1)^n 2^n}{(2n+3)!!} (\beta' S^2)^{n+1} \\ &= \frac{2}{9} \frac{\hbar^2 S^2}{k_B T} \left(1 - \frac{2}{5} \beta' S^2 + \frac{4}{35} (\beta' S^2)^2 + \dots\right) \\ &< \frac{2}{9} \frac{\hbar^2 S^2}{k_B T}, \end{aligned} \quad (\text{A6})$$

where $\beta' = \hbar^2/2\mathcal{J}k_B T$.

APPENDIX B: THE SECOND-ORDER CUMULANT FOR THE DECOUPLING REGIME

The ensemble average of the second-order cumulant is determined by $\langle \hat{S}_z \rangle^2$ of each level in the magnetic field and the energy in the absence of a magnetic field. We first calculate the wave function in the decoupling region using the perturbation for the coupling.

According to Eq. (50), the coupling is much weaker than the magnetic field. If the coupling were to vanish, the superspin is completely decoupled from the cluster and precesses about the direction of the magnetic field independently of the rotor. Thus, the wave function of superspin becomes $|S\sigma\rangle$, and one of the clusters is a linear combination of $\mathcal{D}_{\mu k}^R(\Omega)$ for intrinsic quantum number k . The total wave function is constructed as a direct product of them.

The actual wave function is not decoupled but perturbed by the weak coupling. The matrix element of the coupling Hamiltonian of degenerate space $(H_{\text{coupl}})_{k,k'}^{R\mu\sigma}$ can be calculated as

$$(H_{\text{coupl}})_{k,k'}^{R\mu\sigma} = A_{\kappa} \langle Rk4\kappa | Rk' \rangle \langle R\mu40 | R\mu \rangle \langle S\sigma40 | S\sigma \rangle. \quad (\text{B1})$$

According to the perturbation theory for degenerate case, the unperturbed base $\Psi_{RM\sigma\nu}^{(0)}$ is obtained as the eigenstates of $(H_{\text{coupl}})_{k,k'}^{R\mu\sigma}$:

$$\Psi_{RM\sigma\nu}^{(0)} = \sqrt{\frac{2R+1}{8\pi^2}} c_k^{\nu} \mathcal{D}_{\mu k}^R(\Omega) \otimes |S\sigma\rangle, \quad M = \mu + \sigma. \quad (\text{B2})$$

We further take into account the coupling up to the second-order perturbation. If we apply second-order perturbation naively, the wave function (B2) is mixed with the state of different σ and one in different R . But we can neglect the mixing with states in different R because of Eq. (51) in which the energy differences between states of different R are much larger than the magnetic field. The perturbed wave function $\Psi_{RM\sigma\nu}^{(2)}$ can be evaluated as

$$\begin{aligned} \Psi_{RM\sigma\nu}^{(2)} &= \left\{ 1 - \frac{u_B^2}{2} \sum_{\sigma \neq \sigma'} \frac{|\langle \Psi_{RM\sigma'\nu'}^{(0)} | H_C | \Psi_{RM\sigma\nu}^{(0)} \rangle|^2}{(\sigma - \sigma')^2} \right\} \Psi_{RM\sigma\nu}^{(0)} \\ &+ u_B \sum_{\sigma \neq \sigma'} \frac{\langle \Psi_{RM\sigma'\nu'}^{(0)} | H_C | \Psi_{RM\sigma\nu}^{(0)} \rangle}{(\sigma - \sigma')} \Psi_{RM\sigma'\nu}^{(0)} \\ &+ u_B^2 \sum_{\sigma \neq \sigma'} (\text{const}) \Psi_{RM\sigma'\nu}^{(0)}, \end{aligned} \quad (\text{B3})$$

where $u_B = u'/Bg_s\hbar$ and $H_C = H_{\text{coupl}}/u'$. Using the perturbed wave function, Eq. (B3), we calculate $\langle \hat{S}_z \rangle^2$ up to second order for the coupling:

$$\frac{\langle \hat{S}_z \rangle^2}{\hbar^2} \simeq \sigma^2 + u_B^2 C_2, \quad (\text{B4})$$

where

$$C_2 = 2\sigma \sum_{\sigma \neq \sigma'} \frac{|\langle \Psi_{RM\sigma'\nu'}^{(0)} | H_C | \Psi_{RM\sigma\nu}^{(0)} \rangle|^2}{(\sigma' - \sigma)}.$$

The energy in the absence of a magnetic field is also treated as a second-order perturbation of the coupling. The first-order energy shift $u' \epsilon_{\nu R}^{(1)}$ is evaluated as the expectation value of H_{coupl} for the unperturbed state:

$$\epsilon_{\nu R}^{(1)} = \langle R\mu 40 | R\mu \rangle \langle S\sigma 40 | S\sigma \rangle \Delta_{\nu R}, \quad (\text{B5})$$

where $\Delta_{\nu R}$ represents the eigenvalue of

$$h_{kk'} = \sum_{\kappa=0,\pm 4} \frac{A_\kappa}{u'} \langle Rk 4 \kappa | Rk' \rangle.$$

We can neglect the second-order energy shift, since the second-order energy shift comes from the mixing with the states in different R .

We calculate the ensemble average of $\langle \hat{S}_z \rangle^2$ using Eq. (B4) and Eq. (B5). The Boltzmann factor is expanded for $u_T = u' / k_B T$. Neglecting terms higher than second order for u_T and u_B , we obtain

$$\frac{\langle \hat{S}_z \rangle_{\text{en av}}^2}{\hbar^2} \simeq \frac{\sum_{R\nu\sigma M} \left[\sigma^2 - u_T \sigma^2 \epsilon_{\nu R}^{(1)} + \left\{ u_B^2 C_2 + \frac{1}{2} u_T^2 \sigma^2 \epsilon_{\nu R}^{(1)2} + \dots \right\} \right] \exp(-\beta E_R)}{\sum_{R\nu\sigma M} \left\{ 1 - u_T \epsilon_{\nu R}^{(1)} + \frac{1}{2} u_T^2 \epsilon_{\nu R}^{(1)2} + \dots \right\} \exp(-\beta E_R)}. \quad (\text{B6})$$

The sum of $\epsilon_{\nu R}^{(1)}$ which is the eigenvalue of $(H_{\text{coupl}})_{k,k'}^{R\mu\sigma}$ vanishes, since $(H_{\text{coupl}})_{k,k'}^{R\mu\sigma}$ is a traceless matrix. Expansion of Eq. (B6) up to second order of u_T and u_B yields

$$\frac{\langle \hat{S}_z \rangle_{\text{en av}}^2}{\hbar^2} \simeq \frac{S(\sigma^2)}{S(1)} + \frac{S(C_2)}{S(1)} u_B^2 + \frac{1}{2} \left(\frac{S(\sigma^2 \epsilon_{\nu R}^{(1)2})}{S(1)} - \frac{S(\epsilon_{\nu R}^{(1)2}) S(\sigma^2)}{S(1)^2} \right) u_T^2, \quad (\text{B7})$$

where $S(x)$ is defined as

$$S(x) = \sum_{R\nu\sigma M} x \exp(-\beta E_R). \quad (\text{B8})$$

Let us estimate the $S(x)$'s appearing in Eq. (B7):

$$S(1) = \sum_R (2S+1)(2R+1)^2 \exp(-\beta E_R), \quad (\text{B9})$$

$$S(\sigma^2) = \sum_R \frac{1}{3} S(S+1)(2S+1)(2R+1)^2 \exp(-\beta E_R). \quad (\text{B10})$$

Before calculating the other $S(x)$'s, we evaluate $\sum_\nu |\Delta_{\nu R}|^2$:

$$\sum_\nu |\Delta_{\nu R}|^2 = \text{Tr}(h_{kk'}^2) = \sum_{\kappa=0,\pm 4} A_\kappa^2 |\langle Rk + \kappa | 4 \kappa Rk \rangle|^2 = \frac{8(2R+1)}{15}. \quad (\text{B11})$$

Substituting Eq. (B11), we make a calculation of the other $S(x)$'s:

$$S(\epsilon_{\nu R}^{(1)2}) = \sum_R \frac{8(2R+1)}{15} \frac{2R+1}{9} \frac{2S+1}{9} \exp(-\beta E_R), \quad (\text{B12})$$

$$S(\sigma^2 \epsilon_{\nu R}^{(1)2}) = \sum_R \frac{8(2R+1)}{15} \frac{2R+1}{9} \frac{(1+2S)[-190+39S(S+1)]}{693} \exp(-\beta E_R), \quad (\text{B13})$$

$$S(C_2) = \sum_R \frac{8(2R+1)}{15} \frac{2R+1}{9} \frac{-8(2S+1)}{9} \exp(-\beta E_R). \quad (\text{B14})$$

Finally, putting Eqs. (B9), (B10), (B12), (B13), and (B14) into Eq. (B7), we obtain the ensemble average of $\langle \hat{S}_z \rangle^2$ as a function of the coupling strength:

$$\langle \hat{S}_z \rangle_{\text{en av}}^2 \simeq \frac{1}{3} \hbar^2 S(S+1) - \frac{64}{1215} \left(\frac{u'}{B g_s} \right)^2 + \left\{ \frac{4}{135} \hbar^2 \left(\frac{-190+39S(S+1)}{693} \right) - \frac{4}{3645} \hbar^2 S(S+1) \right\} \left(\frac{u'}{k_B T} \right)^2. \quad (\text{B15})$$

- ¹W. de Heer, Paolo Milani, and A. Châtelain, Phys. Rev. Lett. **65**, 488 (1990); Isabelle M. L. Billas, Jorog A. Becker, and Walt A. de Harr, Z. Phys. D **26**, 325 (1993).
- ²J. G. Louderback, A. J. Cox, L. J. Lising, D. C. Douglass, and L. A. Bloomfield, Z. Phys. D **26**, 301 (1993).
- ³J. A. Becker and W. A. de Harr, Ber. Bunsenges. Phys. Chem. **96**, 1237 (1992).
- ⁴D. C. Douglass, A. J. Cox, J. P. Bucher, and L. A. Bloomfield, Phys. Rev. B **47**, 12 874 (1993).
- ⁵D. C. Douglass, J. P. Bucher, and L. A. Bloomfield, Phys. Rev. Lett. **68**, 1774 (1992).
- ⁶A. J. Cox, J. G. Louderback, and L. A. Bloomfield, Phys. Rev. Lett. **71**, 923 (1993).
- ⁷S. E. Apsel, J. W. Emmert, J. Deng, and L. A. Bloomfield, Phys. Rev. Lett. **76**, 1441 (1996).
- ⁸S. N. Khanna and S. Linderoth, Phys. Rev. Lett. **67**, 742 (1991).
- ⁹G. F. Bertsch and K. Yabana, Phys. Rev. A **49**, 1930 (1994).
- ¹⁰G. Bertsch, N. Onishi, and K. Yabana, Z. Phys. D **34**, 213 (1995).
- ¹¹V. Visuthikraisee and G. F. Bertsch, Phys. Rev. A **54**, 5104 (1996).
- ¹²C. Kittel, *Introduction to Solid State Physics*, 6th ed. (Wiley, New York, 1986), p. 429.
- ¹³P. Ballone, Paolo Milani, and W. A. de Heer, Phys. Rev. B **44**, 10 350 (1991).
- ¹⁴A. Bohr and B. R. Mottelson, *Nuclear Structure* (World Scientific, Singapore, 1998), Vol. I, p. 70.
- ¹⁵A. de-Shalit and I. Talmi, *Nuclear Shell Theory* (Academic Press, New York, 1963).